Quantum network of superconducting qubits through an optomechanical interface

Zhang-qi Yin,[1] W. L. Yang,[2] L. Sun,[1] and L. M. Duan[3,1]
[1]*Center for Quantum Information, Institute for Interdisciplinary Information Sciences, Tsinghua University, Beijing 100084, China*
[2]*State Key Laboratory of Magnetic Resonance and Atomic and Molecular Physics, Wuhan Institute of Physics and Mathematics, Chinese Academy of Sciences, Wuhan 430071, China*
[3]*Department of Physics, University of Michigan, Ann Arbor, Michigan 48109, USA*
(Received 25 July 2014; published 23 January 2015)

We propose a scheme to realize quantum networking of superconducting qubits based on the optomechanical interface. The superconducting qubits interact with the microwave photons, which then couple to the optical photons through the optomechanical interface. The interface generates a quantum link between superconducting qubits and optical flying qubits with tunable pulse shapes and carrier frequencies, enabling transmission of quantum information to other superconducting or atomic qubits. We show that the scheme works under realistic experimental conditions and it also provides a way for fast initialization of the superconducting qubits under 1 K instead of an operation temperature of 20 mK.

DOI: 10.1103/PhysRevA.91.012333 PACS number(s): 03.67.Lx, 42.50.Ex, 42.50.Wk, 85.85.+j

I. INTRODUCTION

Superconducting qubits (SQs) constitute one of the leading candidate systems for realization of quantum computation [1]. Through the circuit resonators, SQs have strong coupling to the microwave photons [1], which can be used for qubit interaction, state engineering of the photonic modes, and nondestructive readout of the qubits [2,3]. Universal quantum logic gates have been realized for SQs in circuit QED (CQED) systems with high fidelity and speed [4]. Through the use of the noise insensitive qubits, the coherent time of the SQs has been increased by several orders of magnitude in recent years and pushed to the 100-μs region [5,6]. In a single circuit resonator, the number of SQs is still limited. Further scaling up the number of qubits requires linking distant CQED systems to form a quantum network. Microwave photons are sensitive to thermal noise and their quantum states only survive under cryogenic temperature. So it is hard to use them to link SQs in two different setups. Optical photons, on the other hand, are robust information carriers at room temperature and serve as ideal flying qubits for long-distance communication. They can carry quantum information to distant locations through an optical fiber.

In this paper we propose a scheme to realize a quantum network of SQs through an optomechanical interface that couples optical photons in a cavity to microwave photons and SQs in a circuit resonator. The interface generates entangled states between SQs and photonic pulses with tunable pulse shape and carrier frequency. The photons then make a quantum link between distant SQs through either a measurement-based entangling protocol or a deterministic state mapping. Because of the tunability of shape and frequency of the emitted photon, the same scheme can also be used to realize a hybrid network between SQs and other matter qubits such as atomic ions [7], quantum dots [8], or defect spins in solids [9]. A hybrid network may allow combination of advantages of different kinds of qubits. For instance, SQs may be good for fast information processing while atomic qubits are ideal for quantum memory. Our scheme is based on the recent advance on the microwave-optical interface: There have been several proposals to realize this interface with ions [10,11], cold atoms [12], or a hybrid optomechanical system with superconducting resonators [13–19] or with a flux qubit [20]. In particular, a recent experiment has demonstrated the transducer between microwave and optical photons using the optomechanical system at a temperature of 4.5 K [21]. One hassle for an interface between SQs and optical photons is that thermal initialization of the SQs requires an operating temperature around 20 mK in a dilution fringe, while an interface to photons requires an optical window, which introduces heating due to blackbody radiation and may significantly increase the system temperature. We circumvent this problem by showing that our proposed scheme can achieve fast initialization of the SQs at 1 K through optical sideband cooling by use of the same optomechanical interface.

II. MODEL

As show in Fig. 1, the system we consider contains an optical cavity (OC) and a microwave superconducting resonator (SR) [22,23], which share an interface that can vibrate and forms a mechanical oscillator (MO) [24,25]. The shared vibrating interface between the OC and the SR has been proposed in several schemes [13–17] and realized very recently in experiments [21,26]. For this system, the MO mode a_m of frequency ω_m couples simultaneously to the optical mode a_1 of frequency ω_1 and the microwave mode a_2 of frequency ω_2. We have assumed that the coupling rate is much less than the mode spacing of either of these oscillators so that only one mode is relevant respectively for the OC, the MO, and the SR. The optical and the microwave modes a_1 and a_2 are driven at the red sideband with frequencies $\omega_{L1} = \omega_1 - \Delta_1$ and $\omega_{L2} = \omega_2 - \Delta_2$, respectively. We set $\Delta_1 = \Delta_2 = \omega_m$. Inside the SR, there are nonlinear Josephson junctions, with the lowest three anharmonic levels shown in Fig. 1(b). The levels $|g\rangle$ and $|s\rangle$ make a SQ, with coupling mediated by the middle level $|e\rangle$ with a coupling rate g_c for the $|g\rangle \rightarrow |e\rangle$ transition and a Rabi frequency $\Omega(t)$ (driven by a microwave field with tunable shape) for the $|e\rangle \rightarrow |s\rangle$ transition.

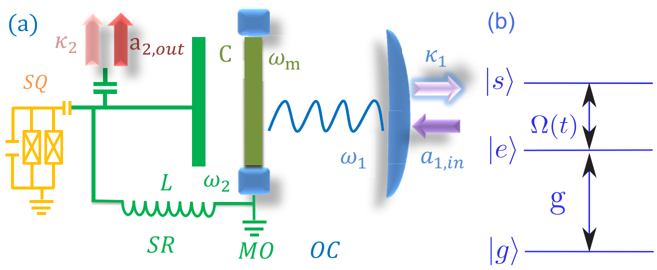

FIG. 1. (Color online) (a) Schematic diagram of the optomechanical quantum interface. The SQ couples with the microwave mode a_2 in a superconducting resonator (SR). The mechanical oscillator (MO) mode a_m for vibration of the interface couples simultaneously to the mode a_2 of the SR and the mode a_1 of the optical cavity (OC). Both modes a_2 and a_1 are driven by coherent classical fields on the red sideband. (b) Energy levels of the superconducting junction, where $|g\rangle$ is the ground state, $|e\rangle$ is the first excited state, and $|s\rangle$ is the second excited state. The transition $|g\rangle$ to $|e\rangle$ couples to the mode a_2 with coupling rate g_c, while transition $|e\rangle$ to $|s\rangle$ is driven by a microwave field with Rabi frequency $\Omega(t)$.

The Hamiltonian of the system has the form $H = H_0 + H_I + H_d$, where

$$H_0 = \sum_{i=1,2} \omega_i a_i^\dagger a_i + \omega_m a_m^\dagger a_m + \omega_e \sigma_{ee},$$

$$H_I = \sum_{i=1,2} g_i a_i^\dagger a_i (a_m + a_m^\dagger) + g_c(\sigma_{eg} + \sigma_{ge})(a_2 + a_2^\dagger),$$

and

$$H_d = \sum_{i=1,2} \left(\frac{\Omega_i}{2} e^{-i\omega_{Li}t} + \text{H.c.}\right)(a_i + a_i^\dagger) + \left(\frac{\Omega'}{2} e^{-i\omega_{L_2}t} + \text{H.c.}\right)(\sigma_{ge} + \sigma_{eg}).$$

We have set $\hbar = 1$ and taken the definition $\sigma_{\mu\nu} = |\mu\rangle\langle\nu|$ ($\mu,\nu = g,e,s$). The SQ and SR drive pulses are generated by two phase-locked microwave generators. The flux control pulses are used to tune the SQ to be resonant with the SR with $\omega_2 = \omega_e$ [23]. The optomechanical coupling rates g_i ($i = 1,2$) are typically small, but their effect can be enhanced through the driving field Ω_i. Under the driving, the steady-state amplitude of the mode a_i is given by $\alpha_i \approx \Omega_i/2\Delta_i$. We take the driving strength $\Omega'^* = g_c\Omega_2/\omega_m$. The optomechanical coupling terms can be expanded with $a_i - \alpha_i$ and the effective coupling Hamiltonian takes the form (see details in Appendix A) [15,16,27]

$$H_{\text{om}} = \sum_{i=1,2} [\omega_m a_i^\dagger a_i + G_i(a_i^\dagger + a_i)(a_m + a_m^\dagger)] + \omega_m a_m^\dagger a_m + (g_c a_2 \sigma_{eg} + \text{H.c.}), \quad (1)$$

where $G_i = \alpha_i g_i$. Under the rotating-wave approximation ($\omega_m \gg G_i, g_c$), the whole Hamiltonian in the interaction picture is given by

$$H_I = (G_1 a_1^\dagger + G_2 a_2^\dagger) a_m + g_c \sigma_{eg} a_2 + \text{H.c.} \quad (2)$$

The corresponding Langevin equations for the a_j ($j = 1,2,m$) modes and the SQ take the form

$$\dot{a}_j = -i[a_j, H_I] - \frac{\kappa_j}{2} + \sqrt{\kappa_j} a_j^{\text{in}},$$
$$\dot{\sigma}_{ge} = -i[\sigma_{ge}, H_I], -\frac{\gamma}{2}\sigma_{ge} + \sqrt{\gamma}\sigma_z a_s^{\text{in}}, \quad (3)$$

where $\sigma_z = \sigma_{ee} - \sigma_{gg}$, γ is the decay rate of the level $|e\rangle$, and κ_j is the decay rate of the mode a_j.

III. SUPERCONDUCTING QUBIT INITIALIZATION AND SQ-PHOTON QUANTUM INTERFACE

Without loss of generality, we take $G_1 = G_2 = G$ for simplicity of notation. We may define the normal modes b and $b_\pm$ with $a_1 = (b_+ + b_- - \sqrt{2}b)/2$, $a_2 = (b_+ + b_- + \sqrt{2}b)/2$, and $a_m = (b_+ - b_-)/\sqrt{2}$, which diagonalize the optomechanical coupling Hamiltonian [28]. The SQ only resonantly couples with normal mode b. The normal mode b decays through two channels a_1^{out} and a_2^{out}. The decay of b mode is denoted by $\kappa = (\kappa_1 + \kappa_2)/2$. Typically, we have $\kappa_1 \gg \kappa_2$, so the photons go out dominantly through the a_1^{out} channel, which is a vacuum. As the SQ only strongly couples with the normal mode b, the steady state of SQ will approach the ground state $|g\rangle$. If the SQ is initially in a mixture of $|g\rangle$ and $|e\rangle$ states, we can cool it to the ground state $|g\rangle$ by driving the red sideband of the optical cavity [29–33]. If the initial state of the SQ involves mixture of other states, these other states can be first driven to the state $|e\rangle$ through a microwave filed and then decay to the ground state $|g\rangle$ by the optomechanical sideband cooling. The working temperature for both initialization and interface can be much higher than tens of mK.

In order to couple the SQ to an output optical photon with controllable pulse shape, we prepare the SQ initially on the level $|s\rangle$ and drive the transition $|s\rangle$ to $|e\rangle$ by a microwave field with Rabi frequency $\Omega(t)$ and pulse duration T_D. The total Hamiltonian of the system is $H_t = H_I + \Omega(t)\sigma_{se} + \text{H.c.}$ In the limit $T_D^{-1} \ll G, g, \kappa_1$, the modes $b_\pm$ are not populated and can be adiabatically eliminated. The effective Hamiltonian is simplified to $H_t = \Omega(t)\sigma_{se} + \frac{\sqrt{2}}{2} g_c b \sigma_{eg} + \text{H.c.}$ The Hamiltonian H_t has a dark state $|D\rangle = [|s\rangle|0\rangle - r(t)|g\rangle|1\rangle]/\sqrt{1 + |r(t)|^2}$, where $r(t) = \sqrt{2}\Omega(t)/g_c$ and $|0\rangle, |1\rangle$ represent the Fock states of the mode b. To solve the output pulse shape, we rewrite the dark state as $|D\rangle = \cos\theta|s\rangle|0\rangle - \sin\theta|g\rangle|1\rangle$, with $\cos\theta = 1/\sqrt{1 + |r|^2}$, and define an orthogonal bright state $|B\rangle = \sin\theta|s\rangle|0\rangle + \cos\theta|g\rangle|1\rangle$. The wave function of the whole system can be expanded as $|\Psi\rangle = (c_d|D\rangle + c_b|B\rangle + c_e|e\rangle) \otimes |\text{vac}\rangle + |g\rangle|0\rangle \otimes |\varphi\rangle$, where $|\text{vac}\rangle$ is the vacuum state of output field and $|\varphi\rangle = \int_{-\omega_c}^{+\omega_c} d\omega\, c_\omega a_{\text{out}}^\dagger(\omega)|\text{vac}\rangle$ denotes the single-photon state of the output field with frequency spectrum c_ω. The dynamics of the system is determined by the Schrödinger equation $i\partial_t|\Psi\rangle = H_t|\Psi\rangle$, where H_t is the total Hamiltonian that includes the input-output coupling terms [34]. Using the method in Ref. [34], the output pulse shape $f(t)$, given by the Fourier transform of c_ω, can be solved analytically in the adiabatic limit, with

$$f(t) = \sqrt{\kappa}\sin\theta \exp\left(-\frac{\kappa}{2}\int_0^t \sin^2\theta(\tau)d\tau\right). \quad (4)$$

The pulse shape $f(t)$ is fully determined by $\theta(t)$.

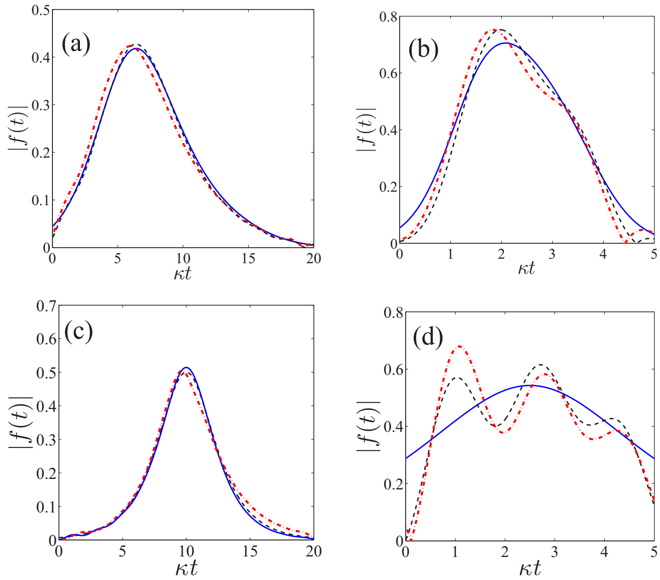

FIG. 2. (Color online) (a) Shape of the output single-photon pulse $|f(t)|$. We take $g = G = 3\kappa$ and the pulse duration $T_D = 20/\kappa$. The driving pulse $\Omega(t) = ge^{-(t-T_D/2)^2/2t_w^2}$ is assumed to be a Gaussian shape with the peak at $t = T_D/2$ and a width $t_w = T_D/5$. The solid, dashed, and dash-dotted curves represent the analytic pulse shape in Eq. (4) derived in the adiabatic limit, the numerical result that includes the contribution of the bright state $|B\rangle$, and the exact result that includes contributions of all the modes $b,b_\pm$, respectively. The shape function is normalized according to $\int |f(t)|^2 dt = 1$ for the convenience of comparison. The overlap between the exact shape (dash-dotted curve) and the adiabatic shape (solid curve) is about 99%. (b) Same as (a) but with the pulse duration $T_D = 5/\kappa$. The adiabatic approximation is not well satisfied in this case and the shape overlap is reduced to 80%. (c) Same as (a) but with the driving Rabi frequency $\Omega(t) = (g_c/\sqrt{2})e^{\kappa(t-T_D/2)/2}$, which gives a symmetric output pulse shape [34]. In the adiabatic limit, the shape (solid curve) is given by the analytic form $f(t) = \sqrt{\kappa/4}\,\mathrm{sech}[\kappa(t - T_D/2)/2]$, which has an overlap of 99.7% with the exact shape. (d) Same as (c) but with the pulse duration $T_D = 5/\kappa$.

To check whether the pulse shape of Eq. (4) derived under the adiabatic limit holds under typical experimental parameters, we compare in Fig. 2 the pulse shapes obtained from the analytic formula and from the exact numerical simulation. In numerical simulation, we solve the exact system dynamics by including the contribution of populations either in the bright state $|B\rangle$ or of all three modes b and $b_\pm$. As one can see from Fig. 2, if the pulse duration $T_D \gtrsim 20/\kappa$, the pulse shape from the analytic formula (4) overlaps very well with the exact result, with the mismatching error less than 1%. However, for a short pulse with $T_D \sim 5/\kappa$, there is a significant shape mismatching error and one should use the exact result instead of the approximate analytic formula. The exact result shows some oscillations in the pulse shape for a short driving field, resulting from the population oscillation in different modes b and $b_\pm$ when the condition of adiabatic elimination $T_D^{-1} \ll G,g,\kappa_1$ is not well satisfied.

IV. QUANTUM NETWORKING OF SQS

In the above we have shown how to couple a SQ to a single optical output photon with a controllable pulse shape. This ability is critical for building up a quantum network of SQs or a hybrid network between SQs and other matter qubits. Here we mention two complementary schemes for quantum networking of SQs, requiring different kinds of pulse shape control.

The key requirement of quantum networking is to generate entanglement between remote SQs. The first scheme for entanglement generation is based on a deterministic quantum state transfer between SQs in two remote cavities [35]. As absorption is the time reversal of the emission process, it has been shown in Ref. [35] that an emitted single-photon pulse can be completely absorbed by a matter qubit in a cavity if we simultaneously reverse the temporal shape of the photon pulse and the driving filed $\Omega(t)$. As shown in Fig. 2, with an appropriate control of the driving microwave field $\Omega(t)$, we can transfer a quantum state from a SQ to a single-photon pulse with a symmetric temporal shape. This single-photon pulse, after propagation in an optical fiber, can then be absorbed by a SQ in another remote cavity, if the driving $\Omega'(t)$ of the second SQ is the time reversal of $\Omega(t)$. The shape control of the driving microwave pulse $\Omega(t)$ or $\Omega'(t)$ can be easily achieved through modulation by an arbitrary wave form generator. If we make a half transfer of the population from the first SQ to the photonic pulse, the generated state between the SQ and the output photon p has the form $(|s\rangle_1|0\rangle_p + |g\rangle_1|1\rangle_p)/\sqrt{2}$. Then, after absorption of the photon by the second SQ, we generate an entangled state $(|s\rangle_1|g\rangle_2 + |g\rangle_1|s\rangle_2)/\sqrt{2}$ between two remote SQs, as required for quantum networking.

The entanglement between remote SQs can also be generated in a probabilistic fashion through detection of interference of the emitted photon(s) [34,36,37]. For instance, as shown in Fig. 4(a), we have SQs in two remote cavities, each emitting a single-photon pulse with a small probability $p_0 = 1 - \exp[-\kappa \int_0^{T_D} \sin^2\theta(\tau)d\tau]$ through an incomplete adiabatic passage from the state $|s\rangle$ to $|g\rangle$. The emitted pulses, after propagation in optical channels, interfere at a 50%-50% beam splitter, with outputs detected by single-photon counters. If we register only one photon from these detectors, the two SQs are projected to an entangled state $(|s\rangle_1|g\rangle_2 + e^{i\varphi}|g\rangle_1|s\rangle_p)/\sqrt{2}$ with a success probability proportional to $p_0 \ll 1$. The unknown relative phase φ can be canceled during the detection process [38] or through the second round of entanglement generation by applying the same protocol again [39]. Compared with the deterministic scheme [35], this probabilistic scheme has a lower efficiency as the protocol needs to be repeated until one successfully registers a photon count, however, it is more robust to noise as the photon loss in the optical channels does not influence the fidelity of this scheme.

A major challenge for quantum networking based on the photonic connection is to achieve the spectrum (shape) and frequency matching of the emitted photon pulses from different matter qubits. For solid-state qubits in particular, the coupling parameters usually vary for different systems and it is hard to get identical qubits or coupling rates. A remarkable advantage of the scheme based on the optomechanical interface is that

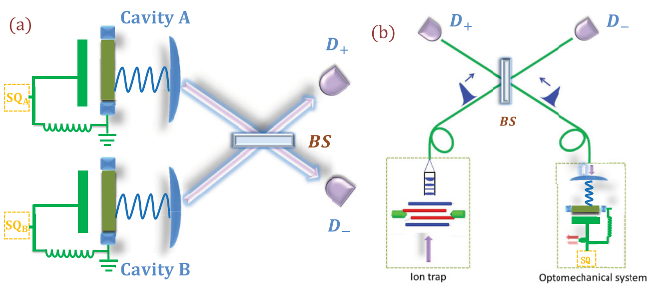

FIG. 3. (Color online) (a) Schematic to generate entanglement between remote SQs. Two SQs are located in distant cavities A and B. The SQs with dashed boxes represent the same structure as the orange part (SQ) in Fig. 1(a), capacitively coupled to the SRs. The SQs couple to the output photons through optomechanical interfaces. The output photons, after propagation, interfere at a beam splitter and then are detected by single-photon counters. Registration of a photon count generates entanglement between the remote SQs. (b) The same setup can be used to entangle SQs with other kinds of matter qubits, such as trapped ions. The carrier frequency and shape of the photon from the SQ is tuned by the optomechanical interface to match with the photon pulse from other matter qubits.

all the mismatches in frequencies or pulse shapes can be easily compensated through the driving fields. For instance, the scheme works perfectly well if the coupling or decay rates are different for different systems. As the pulse shape only depends on $\theta(t)$ from Eq. (4), we can always get identical shapes as difference in the coupling rates can be easily compensated by the microwave driving amplitude $\Omega(t)$. Furthermore, the output optical frequency is purely determined by the eigenmode structure of the optical cavity and not limited by the qubit parameters. So, depending on the frequency and shape of the driving field, we can have a quantum interface between the SQ and the optical photon with widely tunable carrier frequency and shape, which can then interfere with the photons emitted by other kinds of matter qubits, such as trapped ions [40], quantum dots [8,41], or diamond nitrogen vacancy centers [9]. The SQ-optomechanical interface therefore can work as a quantum transducer to generate entanglement links between different types of matter qubits. This leads to a hybrid quantum network, with an example illustrated in Fig. 3(b), which has the important advantage to combine the particular strength of each kind of matter qubits.

V. SUPERCONDUCTING QUBIT INITIALIZATION FIDELITY AND INTERFACE EFFICIENCY

In the above analysis we assume that the SQ couples dominantly to the output field of the optical cavity and neglect other dissipation channels. Now we take into account all the other dissipation processes and calculate their effects on the fidelity of quantum interface. Under the condition that the pulse duration $T_D^{-1} \ll G, g, \kappa_1$, we can adiabatically eliminate all the modes a_j $(j = 1,2,m)$ in the Langevin equations (3) and arrive at the following decay equation for the SQ (see details in Appendix B):

$$\dot{\sigma}_{ge} = -\frac{\gamma_{\rm eff}}{2}\sigma_{ge} + \sqrt{\gamma_{\rm eff}}\sigma_z a_{\rm eff}^{\rm in}, \tag{5}$$

where

$$\gamma_{\rm eff} = \gamma + \tilde{\kappa}_1 + \tilde{\kappa}_2 + \tilde{\kappa}_m,$$
$$a_{\rm eff}^{\rm in} = \left[-i\sqrt{\tilde{\kappa}_1}a_1^{\rm in} + i\sqrt{\tilde{\kappa}_2}a_2^{\rm in} + \sqrt{\gamma}a_s^{\rm in} + \sqrt{\tilde{\kappa}_m}a_m^{\rm in}\right]/\sqrt{\gamma_{\rm eff}},$$
$$\tilde{\kappa}_1 = \frac{4g^2\kappa_1}{(\kappa_1 + \kappa_2 + \kappa_1\kappa_2\kappa_m/4G^2)^2},$$
$$\tilde{\kappa}_2 = \frac{(2 + \kappa_1\kappa_m/2G^2)^2 g^2\kappa_2}{(\kappa_1 + \kappa_2 + \kappa_1\kappa_2\kappa_m/4G^2)^2},$$

and

$$\tilde{\kappa}_m = \frac{g^2\kappa_1^2\kappa_m/G^2}{(\kappa_1 + \kappa_2 + \kappa_1\kappa_2\kappa_m/4G^2)^2}.$$

The physical meaning of Eq. (5) is clear: The SQ couples to four decay channels: the optical channel $a_1^{\rm in}$ with decay rate $\tilde{\kappa}_1$, the microwave channel $a_2^{\rm in}$ with decay rate $\tilde{\kappa}_2$, the mechanical channel $a_m^{\rm in}$ with decay rate $\tilde{\kappa}_m$, and the intrinsic channel $a_s^{\rm in}$ with decay rate γ. For each decay channel, the effective dissipation rate is given by $(\bar{n}_j + 1)\tilde{\kappa}_j$, where $\bar{n}_j = 1/[\exp(\hbar\omega_j/k_B T) - 1]$ is the mean thermal photon (or phonon) number and T denotes temperature of the system. The initialization of the SQ is described by the Langevin equation (5) and the final probability P_g for the SQ in the state $|g\rangle$ is determined by the stationary state under Eq. (5) (after a decay time of the order of $1/\tilde{\kappa}_1 \sim 10$ ns) with

$$P_g = \frac{\tilde{\kappa}_1 + (n_2 + 1)\tilde{\kappa}_2 + (n_m + 1)\tilde{\kappa}_m}{\tilde{\kappa}_1 + (2n_2 + 1)(\gamma + \tilde{\kappa}_2) + (2n_m + 1)\tilde{\kappa}_m}. \tag{6}$$

For the experimental parameters listed in the caption of Fig. 4 and a system temperature of 1 K, the fidelity P_g for state initialization is larger than 99% (we assume temperature $T = 1$ K with $\bar{n}_2 = 1.62$ and $\bar{n}_m = 2.08 \times 10^3$).

For quantum networking of SQs through the optical decay channel, all the other dissipation channels contribute to noise and the fidelity F of the quantum interface can be estimated by the relative ratio of the optical decay rate to the total dissipation

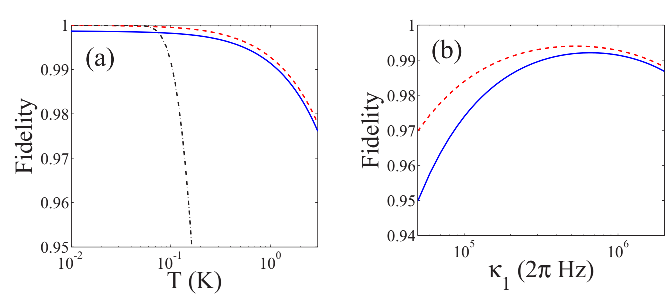

FIG. 4. (Color online) (a) Temperature dependence of the fidelity F (solid curve) of quantum interface and the fidelity P_g (dashed curve) for state initialization. The dash-dotted curve shows the probability in the ground state without optomechanical sideband cooling. The parameters are taken as $\omega_1/2\pi = 200$ THz, $\omega_2/2\pi = 10$ GHz, $\omega_m/2\pi = 10$ MHz [24,25,42], $\kappa_1/2\pi = 10$ MHz, $\kappa_2/2\pi = 1$ kHz, $\kappa_m/2\pi = 10$ Hz [43], $\gamma/2\pi = 5$ kHz [44,45], $G/2\pi = 1$ MHz, and $g_c/2\pi = 1$ MHz. (b) Dependence of the fidelity F (solid curve) and P_g (dashed curve) on the optical cavity decay rate κ_1 at a temperature of 1 K. The other parameters are the same as in (a).

rate

$$F = \frac{\tilde{\kappa}_1}{\tilde{\kappa}_1 + (\bar{n}_2+1)\tilde{\kappa}_2 + (\bar{n}_m+1)\tilde{\kappa}_m + (\bar{n}_2+1)\gamma}, \tag{7}$$

where we have taken $\bar{n}_1 \approx 0$ at the optical frequency. The experimental parameters typically satisfy $G \sim \kappa_1 \gg \kappa_2,\kappa_m,\gamma$. In this case, $\tilde{\kappa}_1 \approx 4g^2/\kappa_1$, $\tilde{\kappa}_2 \approx 4g^2\kappa_2/\kappa_1^2$, and $\tilde{\kappa}_m \approx g^2\kappa_m/G^2$. In Fig. 4 we show the fidelity as a function of the system temperature and the decay rate of the optical cavity. It is found that the fidelity is around 99% for typical values of the experimental parameters as listed in the figure caption.

Typically the SQ system is operated at a temperature around 20 mK, where the ground-state cooling is achieved directly through thermal equilibrium. However, with an optomechanical interface, the system temperature may increase due to heating by the blackbody radiation from the optical window. Here we show that even under a temperature of 1 K, the state can still be initialized through the optomechanical sideband cooling. Another requirement for the system temperature is that the quasiparticle density in the superconducting circuit should be small; otherwise it will induce dissipation of the SQ. The quasiparticle density is proportional to $e^{-1.76T_c/T}$, where T_c is the critical temperature of the superconductor [46]. For niobium, the critical temperature T_c is about 9.3 K, for which the quasiparticle density is negligible at a temperature of 1 K. For aluminum, the T_c is about 1.2 K, where the quasiparticles can be neglected only at temperature on the order of 0.1 K.

VI. CONCLUSION

We have proposed a scheme to realize a quantum network of SQs based on the optomechanical quantum interface. The interface can couple the SQs to optical photons with widely tunable carrier frequencies and pulse shapes. The same interface can also be used for fast initialization of the SQs at a temperature of 1 K through optomechanical sideband cooling.

ACKNOWLEDGMENTS

This work was supported by the National Basic Research Program of China Grants No. 2011CBA00300 and No. 2011CBA00302, and the National Natural Science Foundation of China Grants No. 11105136, No. 11474177, and No. 61435007. W.L.Y. was supported by the National Basic Research Program of China Grant No. 2012CB922102 and by the National Natural Science Foundation of China Grant No. 11274351. L.M.D. acknowledges support from the IARPA MUSIQC program, the ARO, and the AFOSR MURI program.

APPENDIX A: EFFECTIVE LINEAR HAMILTONIAN

The Hamiltonian of the system takes the form $H = H_0 + H_I + H_d$, where

$$H_0 = \sum_{i=1,2} \omega_i a_i^\dagger a_i + \omega_m a_m^\dagger a_m + \omega_e \sigma_{ee},$$

$$H_I = \sum_{i=1,2} g_i a_i^\dagger a_i (a_m + a_m^\dagger) + g_c(\sigma_{eg} + \sigma_{ge})(a_2 + a_2^\dagger),$$

and

$$H_d = \sum_{i=1,2} \left(\frac{\Omega_i}{2} e^{-i\omega_{Li}t} + \text{H.c.}\right)(a_i + a_i^\dagger) + \left(\frac{\Omega'}{2} e^{-i\omega_{L_2}t} + \text{H.c.}\right)(\sigma_{ge} + \sigma_{eg}).$$

The SQ is assumed to couple resonantly with the SR with $\omega_2 = \omega_e$. The detuning $\Delta_i = \omega_i - \omega_{L_i} = \omega_m$. Under the condition that $\Omega_i < 4\omega_i$, the Hamiltonian H_d can be approximated as

$$H_d' = \sum_{i=1,2} \left(\frac{\Omega_i}{2} a_i e^{-i\omega_{Li}t} + \text{H.c.}\right) + \left(\frac{\Omega'}{2} e^{-i\omega_{L_2}t} + \text{H.c.}\right)(\sigma_{ge} + \sigma_{eg}).$$

We take the rotating-wave frame that $H_0' = H_0 - \omega_m(a_1^\dagger a_1 + a_2^\dagger a_2)$. The Hamiltonian in the rotating-wave frame reads

$$H_R = \omega_m \sum_{p=1,2,m} a_p^\dagger a_p + \sum_{i=1,2}\left[g_i a_i^\dagger a_i(a_m + a_m^\dagger) + \left(\frac{\Omega_i}{2} a_i + \text{H.c.}\right)\right] + \omega_e\sigma_{ee} + \left(g_c a_2 e^{-i\omega_{L_2}t} + \frac{\Omega'}{2} e^{-i\omega_{L_2}t} + \text{H.c.}\right)(\sigma_{ge} + \sigma_{eg}). \tag{A1}$$

We assume that the decay rates κ_i for mode a_i $(i = 1,2)$ are much less than the driving detuning $\Delta = \omega_m$. Under the driving, the steady-state amplitude of the mode a_i is given by $\alpha_i \simeq \Omega_i/2\omega_m$. In order to compensate the effect of classical driving on SQ, we set $\Omega'^* = 2\alpha_2 g_c = \Omega_2 g_c/\omega_m$. In the limit that $\alpha_i \gg 1$, the Hamiltonian (A1) can be expanded with $a_i - \alpha_i$,

$$H_{\text{om}} = \sum_{i=1,2} [\omega_m a_i^\dagger a_i + G_i(a_i^\dagger + a_i)(a_m + a_m^\dagger)] + \omega_e\sigma_{ee} + \omega_m a_m^\dagger a_m + (g_c a_2 e^{-\omega_{L_2}t} + \text{H.c.})(\sigma_{eg} + \sigma_{ge}). \tag{A2}$$

Under the rotating-wave approximation $(\omega_m \gg G_i, g_c)$, the whole Hamiltonian in the interaction picture is given by

$$H_I = (G_1 a_1^\dagger + G_2 a_2^\dagger)a_m + g_c\sigma_{eg}a_2 + \text{H.c.} \tag{A3}$$

Here we take the parameters we used in Fig. 4 as an example to make sure that the rotating-wave approximation is valid. In experiments, the typical parameters are as follows: $\omega_1/2\pi = 200$ THz, $\omega_2/2\pi = 10$ GHz, $\omega_m/2\pi = 10$ MHz [24,25,42], $\kappa_1/2\pi = 10$ MHz, $\kappa_2/2\pi = 1$ kHz, $\kappa_m/2\pi = 10$ Hz, $\gamma/2\pi = 5$ kHz [44,45], $g/2\pi = 1$ kHz, and $g_c/2\pi = 1$ MHz. The microwave driving strengths are assumed to be $\Omega_2 = 20$ GHz. The steady-state amplitude $\alpha = 1000$ and $\Omega' = \Omega_2^* g_c^*/\omega_m = 2$ GHz. The effective coupling between a_2 and a_m is $G_2 = \alpha_2 g_2 = 1$ MHz. With proper driving of optical cavity mode a_1, we can also get the effective coupling strength $G_1 = 1$ MHz. Therefore, the rotating-wave-approximation condition $\omega_m \gg G_i, g_2$ is fulfilled.

APPENDIX B: EFFECTIVE LANGEVIN EQUATION FOR THE SQ

In order to derive the effective Langevin equation for the SQ, we write down the Langevin equations of the systems

$$\dot{a}_1 = -iGa_m - \frac{\kappa_1}{2}a_1 + \sqrt{\kappa_1}a_1^{\text{in}}, \tag{B1}$$

$$\dot{a}_2 = -iGa_m + ig\sigma_{\text{ge}} - \frac{\kappa_2}{2}a_2 + \sqrt{k_2}a_2^{\text{in}}, \tag{B2}$$

$$\dot{a}_m = -iG(a_1 + a_2) - \frac{\gamma_m}{2}a_m + \sqrt{\kappa_m}a_m^{\text{in}}, \tag{B3}$$

$$\dot{\sigma}_{ge} = ig\sigma_z a_2 - \frac{\gamma}{2}\sigma_{ge} + \sqrt{\gamma}\sigma_z\sigma_{ge}^{\text{in}}. \tag{B4}$$

In the limit that $G \gg g,\kappa_1,\kappa_2,\kappa_m$, we can adiabatically eliminate modes a_m and $a_{1,2}$. Let us solve a_m from Eq. (B1) in terms of a_1,

$$a_m = \frac{1}{iG}\left(-\frac{\kappa_1}{2}a_1 + \sqrt{\kappa_1}a_1^{\text{in}}\right), \tag{B5}$$

Then we can solve the a_2 from Eq. (B2) in terms of a_1,

$$a_2 = \frac{\kappa_1}{\kappa_2}a_1 - \frac{2}{\kappa_2}\sqrt{\kappa_1}a_1^{\text{in}} + \frac{2ig\sigma_{ge}}{\kappa_2} + \frac{2}{\sqrt{\kappa_2}}a_2^{\text{in}}.$$

Let us solve a_1 from Eq. (B3) and get the expression of a_2,

$$a_1 = \frac{1}{i(G + \gamma_m/\kappa_1 4G)}\left(-iGa_2 + \frac{i\gamma_m}{2G}\sqrt{\kappa_1}a_1^{\text{in}} + \sqrt{\gamma_m}a_m^{\text{in}}\right).$$

Inserting a_1 into the expression of a_2, we get that

$$a_2 = \frac{-8G^2\sqrt{\kappa_1}}{\kappa_2(4G^2 + \kappa_m\kappa_1)}a_1^{\text{in}} - \frac{4iG\kappa_1\sqrt{\kappa_m}}{\kappa_2(4G^2 + \kappa_m\kappa_1)}a_m^{\text{in}} + \frac{2ig\sigma_{ge}}{\kappa_2} + \frac{2}{\sqrt{\kappa_2}}a_2^{\text{in}}. \tag{B6}$$

We get that

$$a_2 = \frac{1}{4G^2(\kappa_1 + \kappa_2) + \gamma_m\kappa_1\kappa_2}\big[-8G^2\sqrt{\kappa_1}a_1^{\text{in}} - 4iG\kappa_1\sqrt{\kappa_m}a_m^{\text{in}} + (8G^2 + 2\kappa_m\kappa_1)\sqrt{\kappa_2}a_2^{\text{in}} + i(8G^2 + 2\kappa_m\kappa_1)g\sigma_{ge}\big]. \tag{B7}$$

Finally, we get that the effective Langevin equation for σ_{ge} is

$$\dot{\sigma}_{ge} = -\left(\frac{2g^2 + g^2\kappa_m\kappa_1/2G^2}{(\kappa_1 + \kappa_2) + \kappa_m\kappa_1\kappa_2/4G^2} + \frac{\gamma}{2}\right)\sigma_{ge} + \frac{-2ig\sqrt{\kappa_1}\sigma_z}{(\kappa_1 + \kappa_2) + \kappa_m\kappa_1\kappa_2/4G^2}a_1^{\text{in}} + \frac{i(2 + \kappa_m\kappa_1/2G^2)g\sqrt{\kappa_2}\sigma_z}{(\kappa_1 + \kappa_2) + \kappa_m\kappa_1\kappa_2/4G^2}a_2^{\text{in}} + \frac{g\kappa_1\sqrt{\kappa_m}/G}{(\kappa_1 + \kappa_2) + \kappa_m\kappa_1\kappa_2/4G^2}\sigma_z a_m^{\text{in}} + \sqrt{\gamma}\sigma_z\sigma_{ge}^{\text{in}}. \tag{B8}$$

It is easy to verify that the effective Langevin equation (B8) fulfills the Einstein relation. The effective Langevin equation (B8) for σ_{ge} can be rewritten as

$$\dot{\sigma}_{ge} = -\frac{\gamma_{\text{eff}}}{2}\sigma_{ge} + \sqrt{\gamma_{\text{eff}}}\sigma_z a_{\text{eff}}^{\text{in}}, \tag{B9}$$

where γ_{eff} and $a_{\text{eff}}^{\text{in}}$ are defined as

$$\gamma_{\text{eff}} = \gamma + \frac{16G^2g^2 + 4g^2\kappa_m\kappa_1^2}{4G^2(\kappa_1 + \kappa_2) + \kappa_m\kappa_1\kappa_2}$$

and

$$a_{\text{eff}}^{\text{in}} = \left(\frac{-2ig\sqrt{\kappa_1}}{(\kappa_1 + \kappa_2) + \kappa_m\kappa_1\kappa_2/4G^2}a_1^{\text{in}} + \frac{i(2 + \kappa_m\kappa_1/2G^2)g\sqrt{\kappa_2}}{(\kappa_1 + \kappa_2) + \kappa_m\kappa_1\kappa_2/4G^2}a_2^{\text{in}} + \frac{g\kappa_1\sqrt{\kappa_m}/G}{(\kappa_1 + \kappa_2) + \kappa_m\kappa_1\kappa_2/4G^2}a_m^{\text{in}} + \sqrt{\gamma}a_2^{\text{in}}\right)\Big/\sqrt{\gamma_{\text{eff}}}. \tag{B10}$$

[1] M. H. Devoret and R. J. Schoelkopf, Science **339**, 1169 (2013).

[2] A. Wallraff, D. I. Schuster, A. Blais, L. Frunzio, R.-S. Huang, J. Majer, S. Kumar, S. M. Girvin, and R. J. Schoelkopf, Nature (London) **431**, 162 (2004).

[3] J. Q. You and F. Nori, Phys. Today **58**(11), 42 (2005).

[4] R. Barends *et al.*, Nature (London) **508**, 500 (2014).

[5] H. Paik *et al.*, Phys. Rev. Lett. **107**, 240501 (2011).

[6] J. B. Chang *et al.*, Appl. Phys. Lett. **103**, 012602 (2013).

[7] S. Olmschenk, D. N. Matsukevich, P. Maunz, D. Hayes, L.-M. Duan, and C. Monroe, Science **323**, 486 (2009).

[8] J. R. Schaibley, A. P. Burgers, G. A. McCracken, L.-M. Duan, P. R. Berman, D. G. Steel, A. S. Bracker, D. Gammon, and L. J. Sham, Phys. Rev. Lett. **110**, 167401 (2013).

[9] H. Bernien *et al.*, Nature (London) **497**, 86 (2013).

[10] D. Kielpinski, D. Kafri, M. J. Woolley, G. J. Milburn, and J. M. Taylor, Phys. Rev. Lett. **108**, 130504 (2012).

[11] M. Hafezi, Z. Kim, S. L. Rolston, L. A. Orozco, B. L. Lev, and J. M. Taylor, Phys. Rev. A **85**, 020302(R) (2012).

[12] J. Verdú, H. Zoubi, C. Koller, J. Majer, H. Ritsch, and J. Schmiedmayer, Phys. Rev. Lett. **103**, 043603 (2009).

[13] C. A. Regal and K. W. Lehnert, J. Phys.: Conf. Ser. **264**, 012025 (2011).

[14] J. M. Taylor, A. S. Sørensen, C. M. Marcus, and E. S. Polzik, Phys. Rev. Lett. **107**, 273601 (2011).

[15] Y. D. Wang and A. A. Clerk, Phys. Rev. Lett. **108**, 153603 (2012).

[16] L. Tian, Phys. Rev. Lett. **108**, 153604 (2012).

[17] S. Barzanjeh, M. Abdi, G. J. Milburn, P. Tombesi, and D. Vitali, Phys. Rev. Lett. **109**, 130503 (2012).

[18] Z.-Y. Xue, Z.-q. Yin, Y. Chen, Z. D. Wang, and S.-L. Zhu, arXiv:1301.4139.

[19] K. Zhang, F. Bariani, Y. Dong, W. Zhang, and P. Meystre, arXiv:1410.0070.

[20] K. Xia, M. R. Vanner, and J. Twamley, Sci. Rep. **4**, 5571 (2014).
[21] R. W. Andrews *et al.*, Nat. Phys. **10**, 321 (2014).
[22] F. R. Ong, M. Boissonneault, F. Mallet, A. Palacios-Laloy, A. Dewes, A. C. Doherty, A. Blais, P. Bertet, D. Vion, and D. Esteve, Phys. Rev. Lett. **106**, 167002 (2011).
[23] A. Dewes, F. R. Ong, V. Schmitt, R. Lauro, N. Boulant, P. Bertet, D. Vion, and D. Esteve, Phys. Rev. Lett. **108**, 057002 (2012); A. Dewes, R. Lauro, F. R. Ong, V. Schmitt, P. Milman, P. Bertet, D. Vion, and D. Esteve, Phys. Rev. B **85**, 140503(R) (2012).
[24] J. D. Teufel *et al.*, Nature (London) **475**, 359 (2011).
[25] J. D. Teufel *et al.*, Nature (London) **471**, 204 (2011).
[26] O. Suchoi, K. Shlomi, L. Ella, and E. Buks, arXiv:1408.2331.
[27] Z.-q. Yin and Y.-j. Han, Phys. Rev. A **79**, 024301 (2009).
[28] Z.-q. Yin and F.-l. Li, Phys. Rev. A **75**, 012324 (2007); Z.-q. Yin, F.-l. Li, and P. Peng, *ibid.* **76**, 062311 (2007).
[29] I. Wilson-Rae, N. Nooshi, W. Zwerger, and T. J. Kippenberg, Phys. Rev. Lett. **99**, 093901 (2007).
[30] F. Marquardt, J. P. Chen, A. A. Clerk, and S. M. Girvin, Phys. Rev. Lett. **99**, 093902 (2007).
[31] Z.-q. Yin, Phys. Rev. A **80**, 033821 (2009).
[32] Z.-q. Yin, T. Li, and M. Feng, Phys. Rev. A **83**, 013816 (2011).
[33] Y.-C. Liu *et al.*, Chin. Phys. B **22**, 114213 (2013).
[34] L. M. Duan, A. Kuzmich, and H. J. Kimble, Phys. Rev. A **67**, 032305 (2003).
[35] J. I. Cirac, P. Zoller, H. J. Kimble, and H. Mabuchi, Phys. Rev. Lett. **78**, 3221 (1997).
[36] S. D. Barrett and P. Kok, Phys. Rev. A **71**, 060310(R) (2005).
[37] C. Galland *et al.*, Phys. Rev. Lett. **112**, 143602 (2014).
[38] C. W. Chou *et al.*, Nature (London) **438**, 828 (2005).
[39] L. M. Duan, M. Lukin, J. I. Cirac, and P. Zoller, Nature (London) **414**, 413 (2001).
[40] L.-M. Duan and C. Monroe, Rev. Mod. Phys. **82**, 1209 (2010).
[41] W. B. Gao, P. Fallahi, E. Togan, J. Miguel-Sanchez, and A. Imamoglu, Nature (London) **491**, 426 (2012).
[42] J.-M. Pirkkalainen *et al.*, Nature (London) **494**, 211 (2013).
[43] T. A. Palomaki *et al.*, Nature (London) **495**, 210 (2013).
[44] C. Rigetti *et al.*, Phys. Rev. B **86**, 100506(R) (2012).
[45] M. Reagor *et al.*, Appl. Phys. Lett. **102**, 192604 (2013).
[46] J. Bardeen, L. N. Cooper, and J. R. Schrieffer, Phys. Rev. **106**, 162 (1957).